Iron and redox sensing in plants: properties of the hemerythrin-like domains of Arabidopsis BRUTUS and BRUTUS-LIKE2 proteins

Authors: Jacob Pullin[1], Jorge Rodríguez-Celma[2], Marina Franceschetti[1], Julia E A Mundy[1], Dimitri A Svistunenko[3], Justin M Bradley[4], Nick E Le Brun[4] and Janneke Balk[1,5]*

[1] Department of Biochemistry and Metabolism, John Innes Centre, Norwich NR4 7UH, UK
[2] Plant Biology Department, Estación Experimental de Aula Dei (EEAD), CSIC, 50059 Zaragoza, Spain
[3] School of Life Sciences, University of Essex, Colchester, Essex CO4 3SQ, UK
[4] Centre for Molecular and Structural Biochemistry, School of Chemistry, University of East Anglia, Norwich Research Park, Norwich NR4 7TJ, UK
[5] School of Biological Sciences, University of East Anglia, Norwich NR4 7TJ, UK

* Author for correspondence, janneke.balk@jic.ac.uk

ABSTRACT

Iron uptake in plants is negatively regulated by a unique subfamily of ubiquitin E3 ligases, exemplified by *Arabidopsis thaliana* BRUTUS (BTS). These large proteins are comprised of an usual triple hemerythrin (Hr)-like domain at the N-terminus and a RING-type E3 ligase at the C-terminus. Physiological studies point to the highly conserved BTS proteins as the elusive iron sensors in plants, but biochemical evidence for this has been lacking. Here we characterize the redox properties and iron-binding dynamics of the Hr-like domain in both BTS and BTS-LIKE2 (BTSL2) and propose a model for their atypical mechanism of iron sensing. The recombinantly expressed BTS N-terminal domain contained three diiron centres, one in each Hr-like motif, whereas BTSL2 lacked the second diiron centre, which is positioned at the distal end according to protein models and SAXS data. The diiron centres of BTSL2 were reduced by dithionite and glutathione and could be re-oxidized upon exposure to O_2 and H_2O_2. In the reduced state, at least one of the irons of each diiron centre was labile and readily accessible to an Fe^{2+} chelator. Addition of Fe^{2+} to the hemi-apoprotein form and subsequent oxidation reconstituted the diiron centres, as monitored by circular dichroism spectroscopy. In the oxidized state, none of the Fe^{3+} ions were labile. These data show that iron binding to BTS/L is dynamic, in support of their proposed iron-sensing function, but interestingly it is conditional on O_2 or oxidative stress. We speculate that the dual-sensing mode may be particularly important for photosynthetic organisms, for which labile diiron centres rather than other iron cofactors have been selected during evolution.

INTRODUCTION

The concentration of iron in cells and whole organisms is tightly controlled to meet demands while avoiding toxicity from redox cycling of free iron (Fenton chemistry). In plants, the uptake of iron is negatively regulated by specific ubiquitin E3 ligases, known as Hemerythrin RING and Zinc-finger (HRZ) proteins in monocots, and named BRUTUS (BTS) in dicot species [1]. The related BTS-LIKE (BTSL) proteins are found in dicots only and have a specific role in regulating iron uptake in roots [2,3]. Mutations in the rice *HRZ* or Arabidopsis *BTS* genes result in accumulation of excessive amounts of iron, leading to embryo lethality in knockout alleles [4-6]. By contrast, Arabidopsis plants lacking expression of both the *BTSL1* and *BTSL2* genes are viable and accumulate moderate amounts of iron under certain growth conditions [3].

The HRZ/BTS proteins are relatively large (~140 kDa), consisting of consecutive hemerythrin -like sequences at the N-terminus and a RING-type ubiquitin ligase domain at the C-terminus (**Figure 1A**). Despite their name, hemerythrins do not bind heme but a pair of cations, usually iron, and are subdivided into canonical O_2-carrying hemerythrins and hemerythrin (Hr)-like proteins based on the pattern of the metal binding His and Glu residues [7]. The E3 ligase domain of HRZ/BTS interacts with transcription factors orchestrating the iron-deficiency response and targets them for degradation ([8,9] and reviewed in [1]). Combination of a Hr-like sequence and E3 ligase is also found in the mammalian F-box/LRR-repeat protein 5 (FBXL5; [10,11]. FBXL5 has a single Hr-like sequence at the N-terminus and a subunit of a Cullin-type E3 ligase at the C-terminus. In the presence of iron and O_2, FBXL5 promotes interaction with Iron Regulatory Protein 2 (IRP2), followed by ubiquitination and degradation of IRP2 [12]. By analogy, the Hr-like domain of HRZ/BTS has been proposed to sense iron and/or O_2, but no biochemical studies have been reported to date. Moreover, why there are three Hr-like sequences and how redox activity could influence ubiquitin ligase activity are open questions.

Using recombinant protein expression and SAXS, we validated the AlphaFold2 prediction that the three Hr-like folds are tightly packed in the order H2-H1-H3. A range of spectroscopic methods showed that BTS and BTSL2 bind three and two diiron centres, respectively, which are redox-active with O_2 and H_2O_2. The oxidized Hr-like centres bound iron with high affinity, whereas ~60% of the iron was labile upon reduction. These data suggest a model in which BTS/L proteins sense oxidative stress dependent on iron binding, upon which they ubiquitinate their target transcription factors to downregulate iron uptake.

68 RESULTS

69 **The extended N-terminus with three Hr-like sequences is conserved in BTS/L proteins**
70 **throughout the green lineage**

71 Previous phylogenetic analyses identified HRZ/BTS homologues in different clades of the
72 green lineage, including green algae [1,4,13-15]. Similar to higher plants, the expression of algal
73 homologues is induced in response to iron deficiency in *Chlamydomonas reinhardtii*,
74 *Dunaliella* species and diatoms [15], suggesting that the role of HRZ/BTS in iron homeostasis is
75 highly conserved. While most HRZ/BTS protein sequences are predicted to have three
76 sequential Hr-like motifs, homologs with only one or two motifs were reportedly found in some
77 plant genomes using bioinformatics [14]. With the ever-expanding availability and completeness
78 of genome sequences, we revisited the phylogenetic analysis to investigate possible variation
79 in the number of Hr-like motifs. All major groups of angiosperms, ferns, mosses and algae
80 have at least one protein of 1200 - 1400 amino acid residues with 50 - 70% overall sequence
81 similarity to Arabidopsis BTS. The phylogenetic relationship of these proteins follows the
82 accepted evolution of the green lineage (**Figure 1A**). All the investigated HRZ/BTS sequences
83 had an N-terminal sequence over 950 residues in length encompassing three distinct
84 sequences with a predicted alpha-helical bundle fold typical of Hr-like proteins. This includes
85 sequences of HRZ2 in different rice cultivars, indicating that the previously reported open
86 reading frame with one Hr-like sequence was incomplete [4].

87 Surprisingly, HRZ/BTS genes were not found in gymnosperms (conifers, Gingko, etc). This
88 suggests that HRZ/BTS was lost from a gymnosperm ancestor and that this clade uses an
89 entirely different mechanism to suppress iron uptake. However, iron homeostasis has not been
90 studied in this important group of vascular plants.

91 Gene duplication and functional specialization of *HRZ*/*BTS* genes have occurred at least
92 twice: Poaceae (grasses including cereal crops) harbour two *HRZ* paralogues (**Figure 1A**).
93 *HRZ1* and *HRZ2* are very similar in sequence but are functionally non-redundant, as shown
94 by mutant studies in rice [4]. Eudicots including Arabidopsis have an additional monophyletic
95 clade of *BTSL* genes, encoding protein sequences that have diverged substantially from BTS
96 (44% amino acid similarity). Arabidopsis *BTSL1* and *BTSL2* have a more specialized function
97 in regulating iron uptake in roots [1,8], although the precise functional differences with BTS
98 remain to be established.

99 In the main HRZ/BTS clade, all three Hr-like sequences contain the diiron-binding motif H-
100 HxxxE-H-HxxxE (InterPro IPR012312). In the BTSL clade, the second sequence has an
101 incomplete H/E motif but is predicted to have the typcial alpha-helical bundle fold, as

102 previously noted [1]. In some moss sequences, one of the six H/E residues is lacking or not
103 well-aligned (indicated by a question mark in **Figure 1A**).

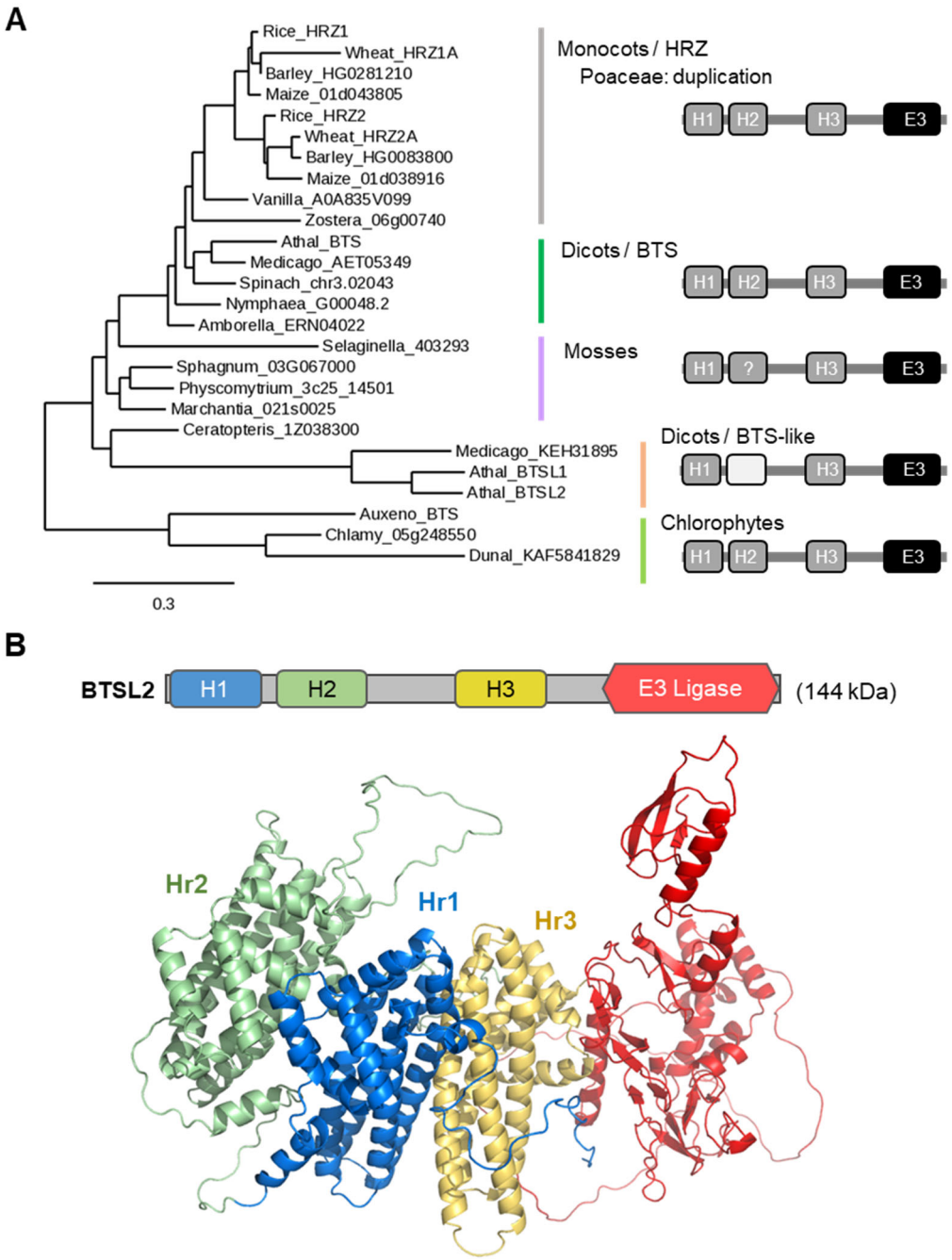

104

105 **Figure 1. Conserved domain organisation of HRZ/BTS proteins and predicted protein fold.**
106 **A**. Phylogeny of HRZ, BTS and BTS-Like (BTSL) proteins from selected organisms across the green
107 lineage (left) and their domain organisation (right). No HRZ/BTS proteins were found in gymnosperms.
108 The hemerythrin (Hr)-like sequences are marked H1, H2 and H3. Dark grey indicates the presence,
109 and light grey the absence, of iron-binding ligands. The question mark indicates that one of the six
110 ligands is absent or not aligned. Abbreviated species names are: Athal, *Arabidopsis thaliana*; Auxeno,
111 *Auxenochlorella protothecoides*; Chlamy, *Chlamydomonas reinhardtii*; Dunal, *Dunaliella salina.*

B. AlphaFold2 model of BTSL2. The Hr-like folds are predicted to be ordered H2–H1–H3 in a tightly packed configuration.

Models of the HRZ/BTS proteins using AlphaFold2 (see examples at www.uniprot.org) consistently show that the three Hr-like folds are arranged in the order H2-H1-H3. There is little interaction between the triple Hr-like domain and the E3 ligase domain, except for the direct connection with H3. The predicted structure is similar for the BTSL2 proteins, as depicted in **Figure 1B**. This places the metal centres, if present, close to one another (~21 Å apart) and arranged in a relatively straight line.

Validation of the triple Hr-like domain fold by SAXS

To obtain experimental evidence for the AlphaFold2 model of the triple Hr-like domain, the N-terminal part of BTSL2 (BTSL2-N, amino acids 1 - 831) from *Arabidopsis thaliana* was produced in *Escherichia coli* for structural studies. The Maltose Binding Protein (MBP) coding sequence was cloned upstream to improve solubility and a Strep tag was added at the C-terminus for affinity purification (**Figure 2A**). Following purification, the MBP-BTSL2-N fusion protein was cleaved with Factor Xa protease and the 98 kDa BTSL-N protein was re-isolated by size-exclusion chromatography (SEC) (**Figure 2B**). Because crystallisation trials were unsuccessful, structural data were obtained through small-angle X-ray scattering (SAXS). This low-resolution technique provides information on the average size and shape of proteins in solution [16]. Scattering is measured as the protein elutes from a SEC column (SEC-SAXS) in a series of frames. This enables selection of the highest quality data, avoiding misfolded and aggregated protein in the sample.

Four frames in the middle of the single elution peak (**Figure S1A**) were selected and merged to give the scattering profile of intensity (I) as a function of q, the momentum transfer variable (**Figure 2C**). The shape of the profile is typical of non-spherical monodispersed particles [16]. Plotting the natural logarithm of intensity, ln(I), versus the square of lower q values, known as Guinier analysis, gave a straight line which confirmed the homogeneity of the sample (**Figure 2C, inset**). The slope of the Guinier plot was used to calculate a radius of gyration R_g of 33.95 ± 0.05 Å. The Bayesian inference method [17] gave a molecular mass of 101 kDa, which is close to the expected molecular mass of 97.771 kDa calculated from the amino acid sequence and shows that the recombinant protein is monomeric. The shape of the Kratky plot of q^2 x I *versus* q (**Figure S1B**) indicated that the particle is globular or globoid with only a small degree of flexibility, in agreement with tight packing of the Hr-like folds.

146 SAXS data can also be assessed in real space using the pair distance distribution function,
147 $P(r)$, which is obtained by indirect Fourier transformation of $I(q)$. The presence of a shoulder
148 in the P(r) distribution (**Figure S1C**) is indicative of the multi-domain structure of BTSL2-N.
149 The maximum distance (D_{max}) determined experimentally was 98 Å, in agreement with the
150 longest predicted axis of 96.5 Å in the AlphaFold2 model. The protein envelope calculated
151 from raw scattering data using DAMMIF software [18] is shown in **Figure 2D,** overlaid with a
152 refined AlphaFold2 model. The χ^2 value of the fit was 1.075. From this we can conclude that
153 the AlphaFold2 structure is representative of the solution structure of BTSL2-N as determined
154 by SAXS.

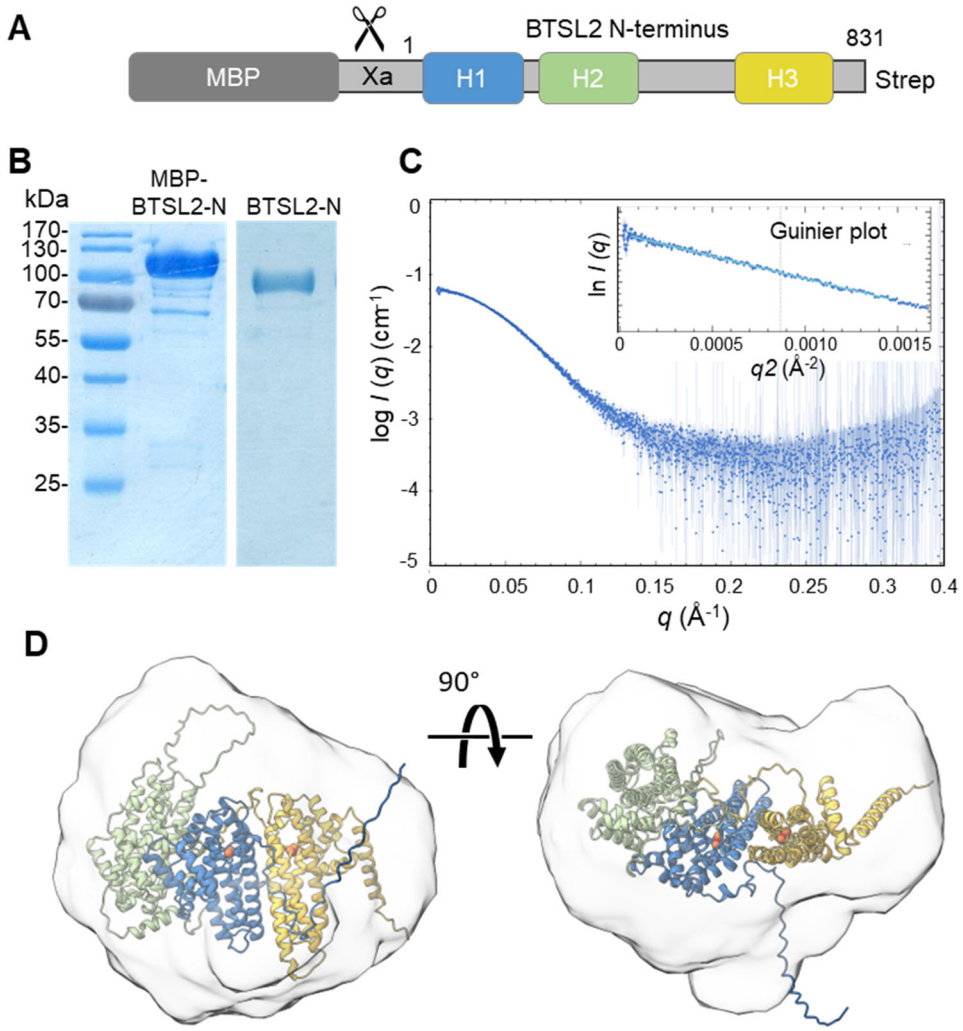

155

156 **Figure 2. Validation of the 3D shape of the BTSL2 Hr-like domain by SAXS.**
157 **A.** Expression construct of the Arabidopsis BTSL2 N-terminus (BTSL2-N, codons 1 – 831)
158 encompassing the three Hr-like sequences, flanked by Maltose Binding Protein (MBP) for solubility and
159 a C-terminal Strep tag for affinity purification. **B.** Coomassie-stained gel of MBP-BTSL2-N purified using
160 Strep-Tactin XT (left) and of BTSL2-N after removal of the MBP domain following protease Xa cleavage
161 and size-exclusion chromatography (right). **C.** Scattering profile of intensity $I(q)$, presented in log-scale,
162 versus q, the momentum transfer variable which is inversely correlated with the X-ray wavelength in

163 Ångstrom ($Å^{-1}$). Inset: Guinier analysis, in which ln(I) is plotted against q^2. A radius of gyration Rg of
164 33.95 ± 0.05 Å was calculated from the slope of the graph (R^2 = 0.9941). The intensity at zero angle
165 $I(0)$ was 0.062 cm^{-1} ± 0.000096 and the residual values showed an even distribution. **D**. Model of the
166 BTSL2-N protein envelope overlaid with a refined AlphaFold2 model with manually inserted diiron
167 centres. Source data have been deposited under accession SASDU79 in www.sasbdb.org.

168

169 **The Hr-like domains of BTSL2 and BTS bind diiron centres, except for H2 in BTSL2**

170 To determine the type and number of metal cofactors in the N-terminal part of BTSL2 and
171 BTS, the purified proteins were analysed by Inductively Coupled Plasma – Mass Spectrometry
172 (ICP-MS) followed by quantitative assays to determine the molar ratio of iron per polypeptide.
173 The MBP domain was not removed to maximize protein yield for these and subsequent
174 analyses (**Figure 3A, B**). For BTS-N, addition of β-mercaptoethanol or glutathione to all
175 buffers was required to prevent precipitation. ICP-MS for a range of transition metals showed
176 that iron was approximately nine times more abundant than zinc or manganese associated
177 with purified MBP-BTS-N, and three times more abundant in purified MBP-BTSL2-N (**Table**
178 **S1**). Using sulfur to estimate the protein concentration, the iron-to-protein ratio was 2.2 for
179 BTS and 3.1 for BTSL2. These numbers are thought to be an underestimation, particularly for
180 BTS, because the sample likely contained residual glutathione.
181
182 Quantitative analysis of iron using a colorimetric reagent and the Bradford assay for protein
183 showed that MBP-BTSL2-N contained 3.9 iron atoms per polypeptide (**Figure 3C**), close to
184 the expected ratio of 4 based on the two predicted diiron binding sites in H1 and H3 (Figure
185 1A). The as-isolated protein was yellow in colour with absorbance around 350 nm, which is
186 typical of diiron proteins (**Figure 3D, E**).

187 To confirm the location of the iron-binding sites, we substituted glutamate (E) in the centre of
188 each H-HxxxE-H-HxxxE motif with alanine (A) by site-directed mutagenesis. This Glu residue
189 bridges canonical diiron centres and E-to-A substitution has previously been shown to
190 completely abolish iron binding at hemerythrin sites [11,19]. E98A substitution in H1 resulted in
191 approximately two iron per polypeptide and a similar result was obtained with the E664A
192 substitution (**Figure 3C**). The single variant proteins were greyish in colour (**Figure 3D**) and
193 had lost most of the absorbance in the 350 nm region (approximately 8000 M^{-1} cm^{-1}, **Figure**
194 **3E**). Combining E98A and E664A decreased the amount of iron associated with BTSL2-N
195 below the detection limit of the colorimetric chelator (**Figure 3C**) despite some residual
196 absorbance (**Figure 3E**).

197 Purified BTS-N contained 5.9 iron atoms per polypeptide (**Figure 3C**), close to the expected
198 ratio of 6 for three diiron centres, one in each Hr-like subdomain. The as-isolated protein was
199 reddish in colour giving a distinct UV-visible spectrum with features at 332 and 420 nm (**Figure**
200 **3D, E**). These are in part reminiscent of an iron-sulfur (Fe-S) cluster, but further spectroscopic
201 analysis ruled out this possibility (see below).

202 These data, together with the structure of the N-terminus, show that BTSL2 lacks a diiron
203 centre in the distally-located H2 and thus has two aligned diiron centres proximal to the E3
204 ligase domain. BTS has a full complement of three diiron centres.

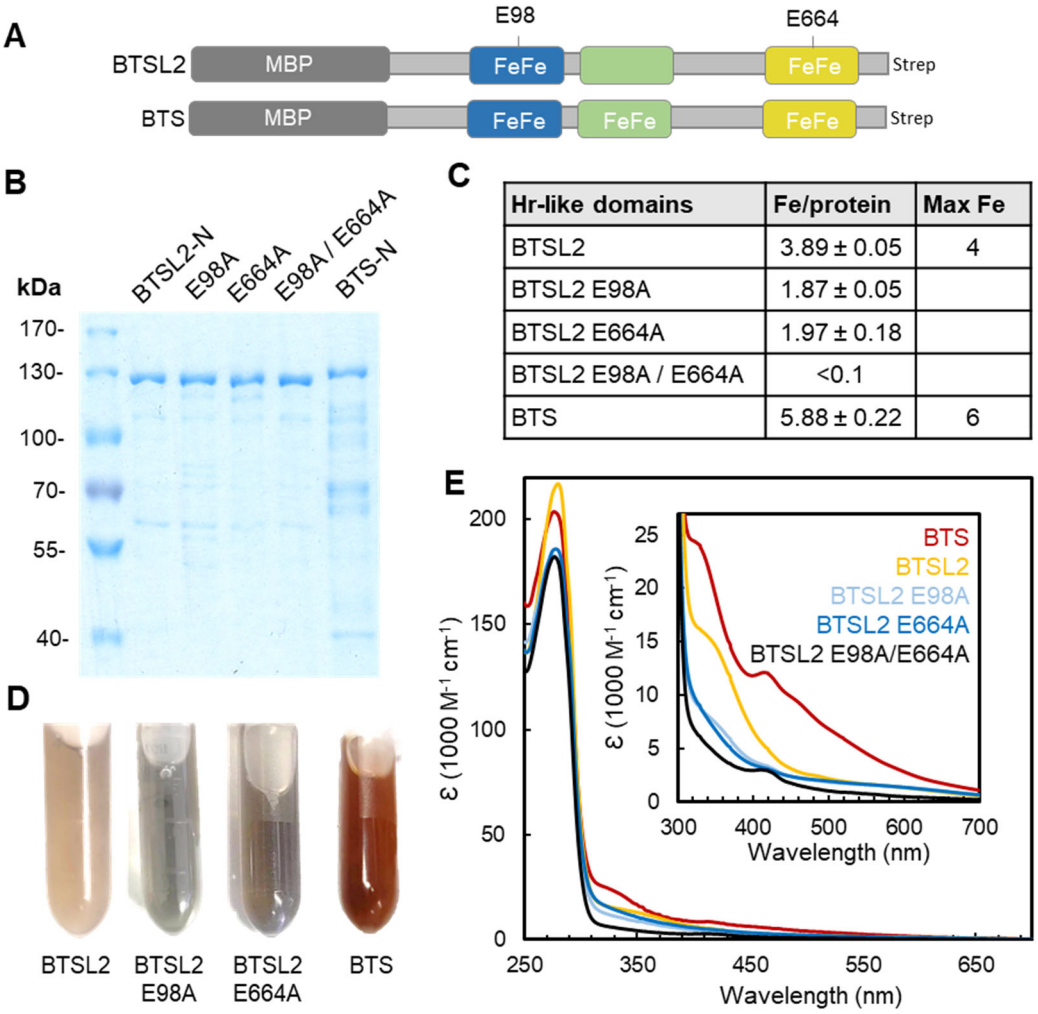

Hr-like domains	Fe/protein	Max Fe
BTSL2	3.89 ± 0.05	4
BTSL2 E98A	1.87 ± 0.05	
BTSL2 E664A	1.97 ± 0.18	
BTSL2 E98A / E664A	<0.1	
BTS	5.88 ± 0.22	6

205

206 **Figure 3. Iron cofactors in the Hr-like domains of BTSL2 and BTS.**
207 **A.** Diagrams of the MBP fusion proteins of Arabidopsis BTSL2 and BTS N-terminal sequences used for
208 iron quantification and spectroscopy. The E98 and E664 residues are indicated. **B**, Coomassie-stained
209 SDS-PAGE gel of the indicated purified proteins including the MBP domain (omitted from the labels).
210 **C.** Quantification of bound iron atoms per polypeptide using the colorimetric chelator Ferene. **D, E.**
211 Colour (C) and UV-visible spectra (D) of the as-isolated proteins from (A). The protein concentrations
212 were BTSL2, 462 μM; BTSL2 E98A, 345 μM; BTSL2 E664A, 527 μM; BTS, 222 μM.

213 **The Hr-like iron centres react with O_2 and H_2O_2**

214 Next, we investigated whether the Hr-like domains of BTSL2 and BTS are redox-active. The
215 UV-visible spectra of BTSL2-N in Figure 3D indicated that the diiron centres are predominantly
216 in the oxidized, diferric state in the 'as-isolated' protein. Attempts to obtain proteins with diiron
217 centres in a stable reduced state under atmospheric conditions failed, and therefore samples
218 were transferred to an anaerobic chamber where they were mixed with a small excess of
219 sodium dithionite as reductant, followed by buffer exchange on a desalting column to remove
220 dithionite.

221 To probe the reaction with O_2 and H_2O_2, reduced BTSL2-N was titrated with incremental
222 aliquots of oxidant and the changes in UV-visible absorbance were monitored. Following a
223 progressive increase in absorbance in the 320 – 400 nm region (**Figure 4A, B**), addition of a
224 total of 0.25 and 0.5 molar equivalents of O_2 and H_2O_2, respectively, resulted in recovery of
225 the absorbance signals of the as-isolated protein. Changes in the circular dichroism (CD)
226 spectrum showed similar behaviour (**Figure S2**), indicating that BTSL2-N was completely re-
227 oxidized without loss of iron cofactor. Reduction of BTS-N resulted in a less pronounced
228 decrease in absorbance at 320 – 400 nm than for BTSL2-N. Addition of O_2 or H_2O_2 returned
229 the absorbance signals to those of the 'as-isolated' spectrum (**Figure 4D, E**).

230 Based on the concentration of iron in each protein sample and the concentration of oxidant
231 added, the observed stoichiometries of the oxidation reactions were ~0.2 per Fe^{2+} for O_2 and
232 ~0.5 for H_2O_2 (**Figure 4C, F**). These oxidant-to-iron ratios are close to the theoretical minima
233 of 0.25 for O_2 and 0.5 for H_2O_2, and typical for reactions of diiron centres, such as Dps mini-
234 ferritins, bacterioferritin, ribonucleotide reductase or alternative oxidase [20-23], with O_2 and H_2O_2
235 accepting four and two electrons, respectively.

236 To investigate whether the O_2 reaction proceeds via a H_2O_2 intermediate, we probed for H_2O_2
237 formation using the colorimetric dye Amplex Red. Samples of reduced BTSL2-N and BTS-N
238 protein containing 40 μM Fe^{2+} were mixed with air-saturated Amplex Red assay reagents.
239 Following reaction with 20 μM O_2, the theoretical maximum production of H_2O_2 would be 20
240 μM, assuming that all H_2O_2 formed reacted with the Amplex Red reagent. For BTSL2-N and
241 BTS-N, 24.3 and 15.6 μM H_2O_2 were detected, respectively, which is close to the expected
242 amount.

243 We also tested if glutathione could reduce the diiron centres in place of dithionite. A
244 physiological concentration of GSH (3 mM) was mixed with anaerobic BTSL2-N, and we
245 observed reduction of the protein, albeit very slowly (**Figure S3**).

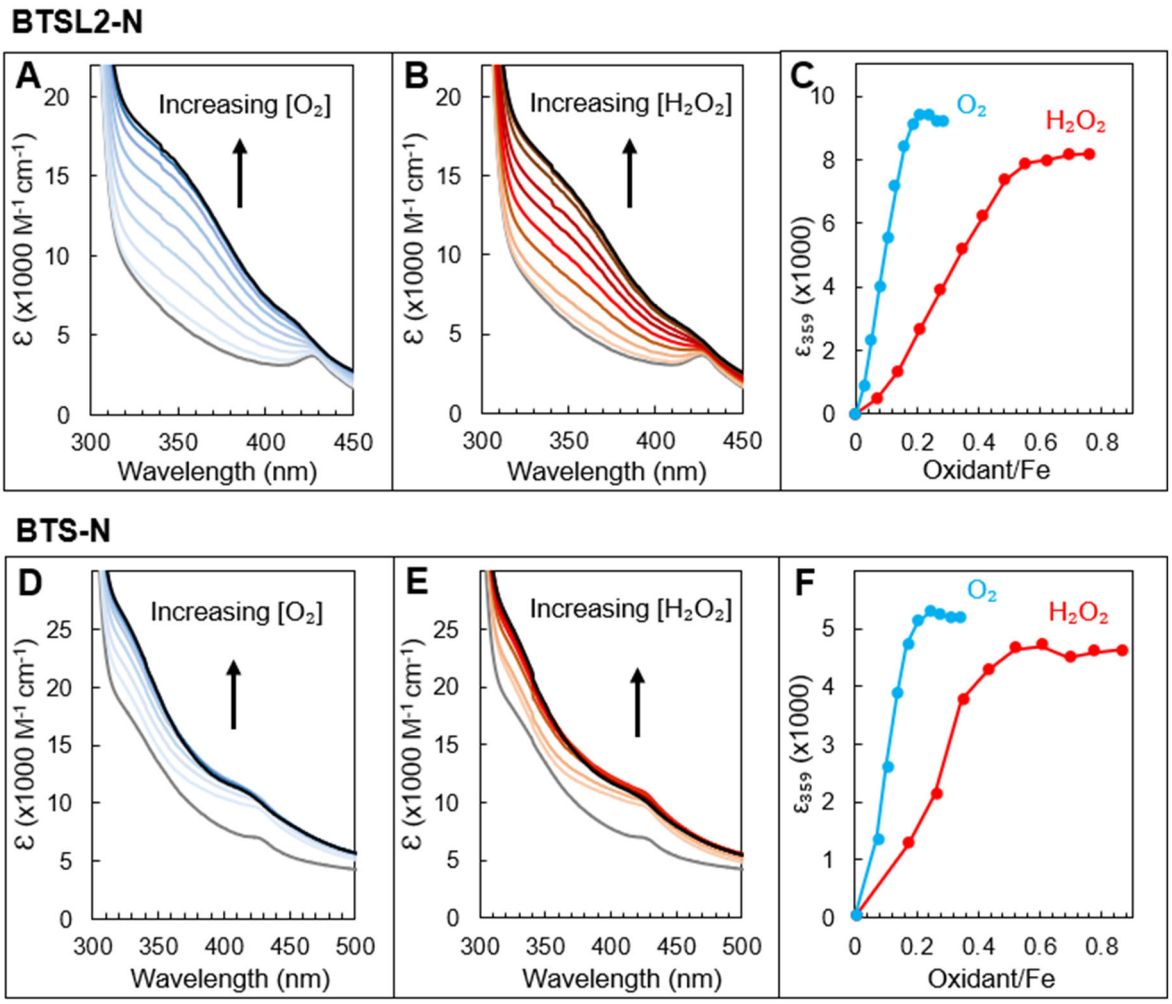

Figure 4. The Hr-like domains of BTSL2 and BTS are redox-active with O_2 and H_2O_2.
A, B, D and E. Redox titrations monitored by UV-visible absorbance spectroscopy of (A, B) 140 μM BTSL2-N and (D, E) 220 μM BTS-N (MBP fusion proteins, see Figure 3). Black line: 'as-isolated' proteins purified in air. Grey line: fully reduced with dithionite in an anaerobic chamber and desalted. Colour lines: titration with O_2 (A and D, blue lines) or H_2O_2 (B and E, orange-red lines). **C, F.** The absorbance at 359 nm as a function of the oxidant to iron ratio based on the spectra in (A) and (B) for BTSL2-N, and spectra in (D) and (E) for BTS-N.

Because the stoichiometry for the reaction with O_2 was somewhat lower than expected, we investigated the possibility that the diiron centres in BTSL2-N and BTS-N were not fully reduced in the presence of excess dithionite, resulting in a proportion of semi-reduced, paramagnetic centres. Electron Paramagnetic Resonance (EPR) spectroscopy of the as-isolated proteins showed a prominent signal at g = 4.3, which was essentially absent from the spectra of the reduced proteins (**Figure 5A, B**). The signal corresponds to mononuclear ferric (Fe^{3+}) iron but represents less than 1% of the total iron in the samples (see quantification described in Materials and Methods). Both BTSL2-N and BTS-N proteins also have a signal

with g-values around 1.9, which can be attributed to a mixed valence Fe^{2+}/Fe^{3+} centre with a μ-oxo bridging ligand rather than a μ-hydroxo-bridged species, which typically has higher g-values [24]. Again, quantification indicated that this species represented less than 1% of the total iron. The overall lack of signal for the majority of the iron is consistent with the expectation that the fully oxidized diiron centres are EPR silent due to antiferromagnetic coupling of the two S = 5/2 Fe^{3+} ions. For BTS-N, which has visible absorbance features at 325 and 420 nm reminiscent of Fe-S clusters, the EPR spectra are clear in ruling out this possibility because there is no specific signal in the reduced protein with g-values typical of Fe-S clusters [25]. Furthermore, CD spectra of BTS/L proteins are also not consistent with those of Fe-S proteins [26-28].

Upon re-exposure to O_2, the g = 4.3 mononuclear iron signal returned to an intensity similar to that of the as-isolated proteins. By contrast, exposure to H_2O_2 resulted in a signal of much lower intensity. The mixed-valence signal was not responsive to oxidant within the timescale of observation, suggesting that this is not a physiologically relevant species. A small EPR signal at g ≈ 2 had features consistent with protein-based peroxyl radicals and was seen inconsistently among some samples; a spectrum of this signal in BTSL2-N is reported on a narrow field range in **Figure S4**.

In summary, UV-visible spectroscopy of protein variants confirmed that there are, respectively, two and three diiron centres in the Hr-like domains of BTSL2 and BTS. EPR spectroscopy rules out the possibility of Fe-S cluster species within the proteins. The diiron centres are redox-active with both O_2 and H_2O_2.

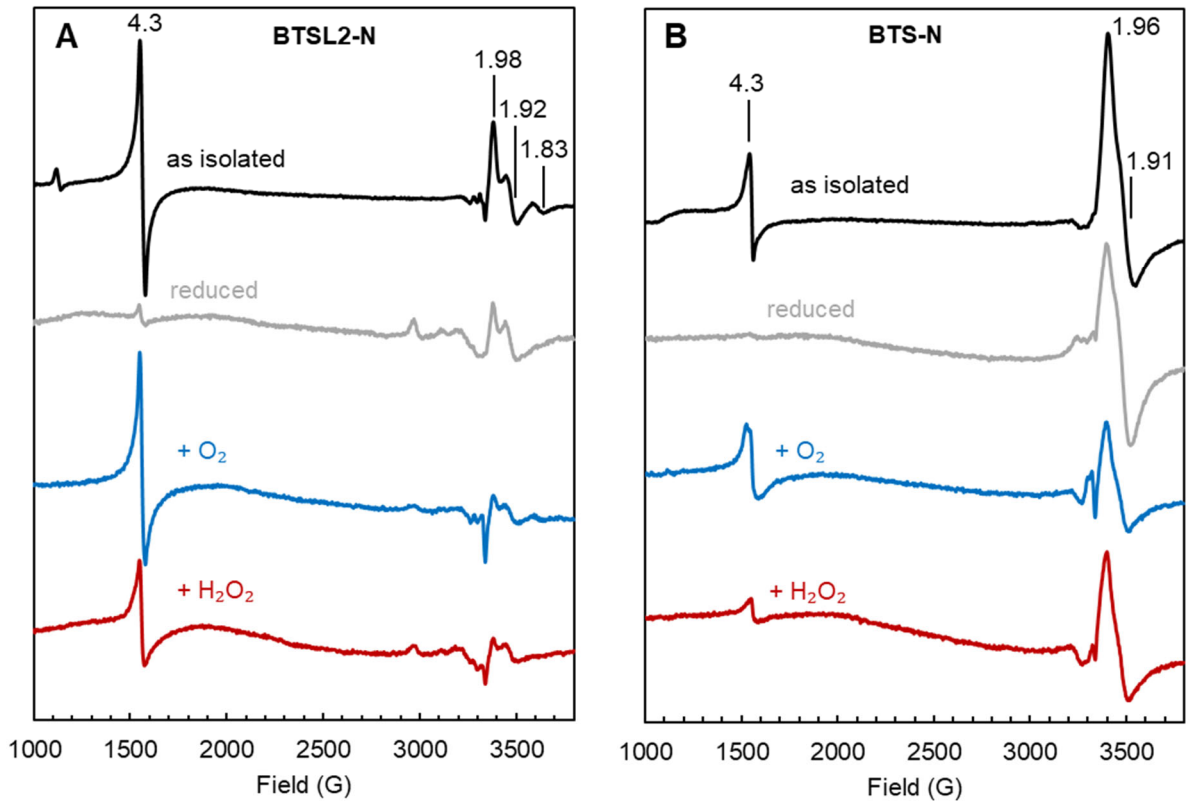

Figure 5. Analysis of protein-bound iron in the Hr-like domains of BTSL2 and BTS by electron paramagnetic resonance (EPR).

EPR spectra of (**A**) BTSL2-N and (**B**) BTS-N. The protein domains were expressed as MBP fusion proteins, see Figure 3A. The signal with g-value 4.3 is mononuclear iron; the signals with g values around 1.9 are characteristic of a mixed valence Fe^{2+}/Fe^{3+} centre. Both signals represent ~1% of the protein-bound iron, because the majority of the diiron centres are EPR silent when fully oxidized or reduced. Black: BTSL2-N (287 μM) and BTS-N (222 μM) proteins as isolated. Grey: BTSL2-N (130 μM) and BTS-N (100 μM) reduced with dithionite and desalted in an anaerobic chamber. Blue: BTSL2-N (106 μM) and BTS-N (84 μM) 3 min after mixing with calculated volumes of supersaturated O_2 solution for end concentrations of 216 μM and 262 μM O_2, respectively. Red: BTSL2-N (106 μM) and BTS-N (84 μM) 3 min after mixing with 216 μM and 262 μM H_2O_2, respectively. Spectra were adjusted to compensate for dilution by reagent additions and desalting. EPR spectra were recorded at 10 K using the following parameters: microwave frequency ν_{MW} = 9.353 GHz, modulation frequency ν_M = 100 kHz, microwave power P_{MW} = 3.17 mW, modulation amplitude A_M = 5 G.

Iron binding to the Hr-like domains of BTSL2 and BTS is reversible in the reduced state

For BTS/L proteins to function as iron sensors, it is expected that they bind iron dynamically. However, iron remained bound to the Hr-like domains of BTSL2 and BTS under the conditions used for purification (Figure 3) and following reduction and re-oxidation (Figure 4). Therefore,

305 we tested if iron chelators can compete with, and extract iron from, BTSL2-N and BTS-N. Iron
306 release was followed in real time by using colorimetric iron chelators such as Ferene
307 (Hennessy et al., 1984). The 'as-isolated', predominantly oxidized form of BTSL2-N displayed
308 a slow but steady rate of approximately 20% iron release per hour when the protein was
309 purified with β-mercaptoethanol in the buffers, or virtually no iron release without β-
310 mercaptoethanol (**Figure 6A**). However, if the iron is released in the ferric form, it may not be
311 detected because Ferene specifically binds Fe^{2+}. To investigate this possibility, we mixed β-
312 mercaptoethanol-free BTSL2-N with the ferric iron chelator ethylenediaminetetraacetic acid
313 (EDTA) and saw no change in the protein's CD spectrum after 1 h (**Figure S5**). Thus, we
314 conclude that, in their oxidized, Fe^{3+} form, the diiron sites are not labile.

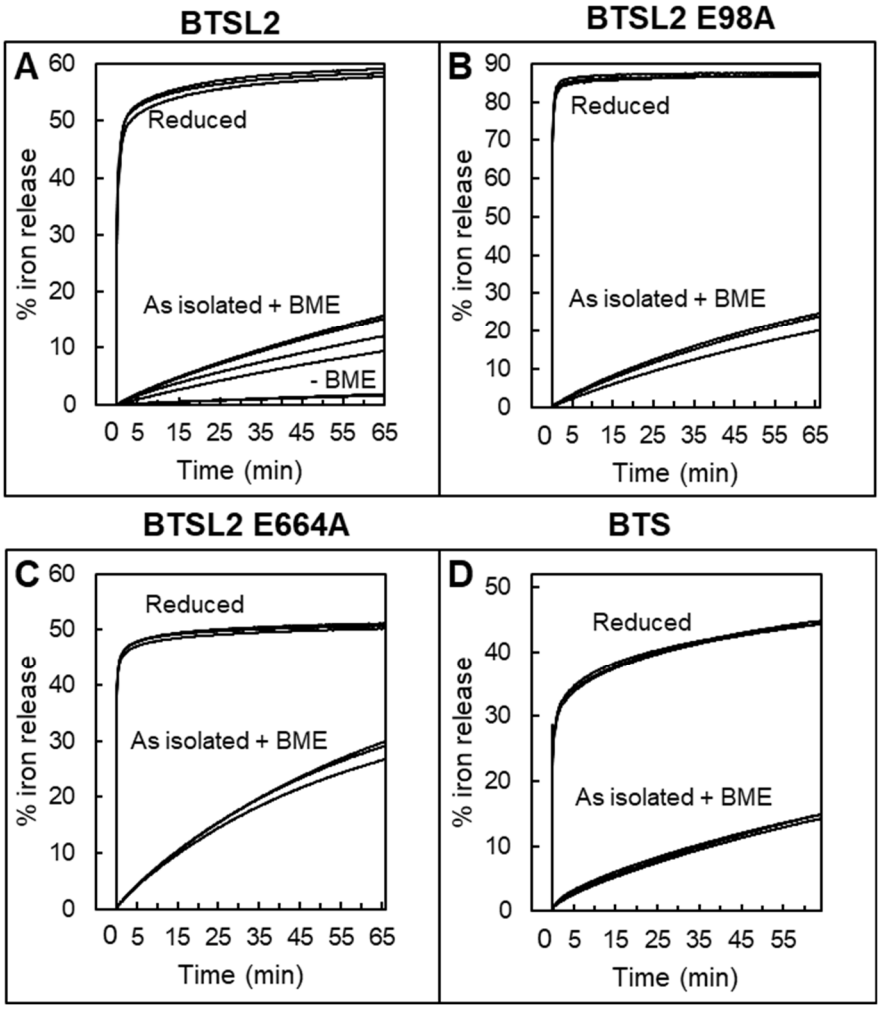

315

316 **Figure 6. Iron binding to the Hr-like domain depends upon oxidation state.**
317 Purified MBP-fusions of the Hr-like domains of BTSL2 and BTS were diluted to an iron concentration of
318 75 μM in sealed cuvettes and mixed with 1 mM of the colorimetric iron chelator Ferene. An increase in
319 absorbance over time was correlated with the amount of iron released from the protein and the rate of
320 release. Proteins were measured "as isolated", which is in the predominantly oxidized form despite the

321 presence of residual β-mercaptoethanol (BME), included to stabilise BTS, or after reduction with
322 dithionite and desalting. **A.** BTSL2-N; **B.** BTSL2-N E98A; **C.** BTSL2-N E664A; **D.** BTS-N.
323
324 Following reduction of BTSL2-N with dithionite and removal of excess reductant, exposure to
325 chelator resulted in release of ~50% of the iron in the first few seconds, and then another 5%
326 more slowly over an hour. For BTS-N, the oxidized sample released ~15% iron over an hour,
327 whereas the reduced protein rapidly released ~30% and then another 20% at a much slower
328 rate (**Figure 6D**). Equivalent experiments with reduced BTSL2-N using two other colorimetric
329 iron chelators, dipyridyl or ferrozine [29,30], gave similar results in terms of the percentage of iron
330 released and the kinetics (**Figure S6**). This demonstrates that the Fe^{2+}-protein dissociation
331 rate, rather than Fe^{2+}-chelator association rate, was measured in these experiments.

332 For both BTSL2-N and BTS-N, not all of the iron was released, indicating that iron in one or
333 more of the diiron centres is not labile, even when reduced. To further investigate this for
334 BTSL2-N, iron release experiments were repeated with the E98A and E664A variant proteins.
335 Reduced E98A BTSL2-N, in which the H3 diiron centre remains intact, released ~85% of the
336 iron in the first rapid phase but did not exhibit the slower release phase observed in the wild-
337 type form (**Figure 6B**). The reduced E664A protein, in which the H1 diiron centre remains
338 intact, released ~45% of its iron, mostly in the rapid first phase (**Figure 6C**). Combining these
339 values equates to a release of 67% iron, which is relatively close to the 60% released from
340 BTSL2-N with both diiron centres. The data indicate that the H3 diiron centre is more labile,
341 releasing up to both irons. The H1 diiron centre is also labile but releases one iron only. In
342 addition, kinetics of both single mutants appear altered relative to the wild-type protein,
343 suggesting that the iron status of one diiron centre affects the other.

344 To investigate whether iron binding is reversible, we tested for re-association of iron after the
345 removal of the 'labile' iron upon addition of Fe^{2+} chelator. The experimental procedure, as
346 outlined in **Figure 7A**, was followed using CD spectroscopy because only protein-bound irn
347 contributes to the spectrum. Under anaerobic conditions, a defined amount of Ferene was
348 added to reduced BTSL2-N to remove 40% of the Fe^{2+} (i.e. less than the proportion removed
349 in the fast phase when excess chelator was added, see Figure 6A). To verify that the iron was
350 indeed removed, half the sample was desalted and oxidized, yielding a CD spectrum with a
351 commensurate decrease in the ellipticity at 350 nm (**Figure 7B**, blue trace). To the other half
352 of the sample, kept under anaerobic conditions, a 3-fold excess of Fe^{2+} in the form of ferrous
353 ammonium sulfate was added followed by a desalting step to remove unbound iron and iron-
354 chelator complexes. After exposure to O_2, the resulting CD spectrum was identical to that of
355 the as-isolated protein (**Figure 7B**, pink trace), indicating full occupancy of the diiron centres
356 and successful re-association of the iron that had been removed. Overall, these data

demonstrate that, in a reducing environment, iron binding to BTS/Ls is reversible. By contrast, in an oxidizing environment, iron remains tightly bound.

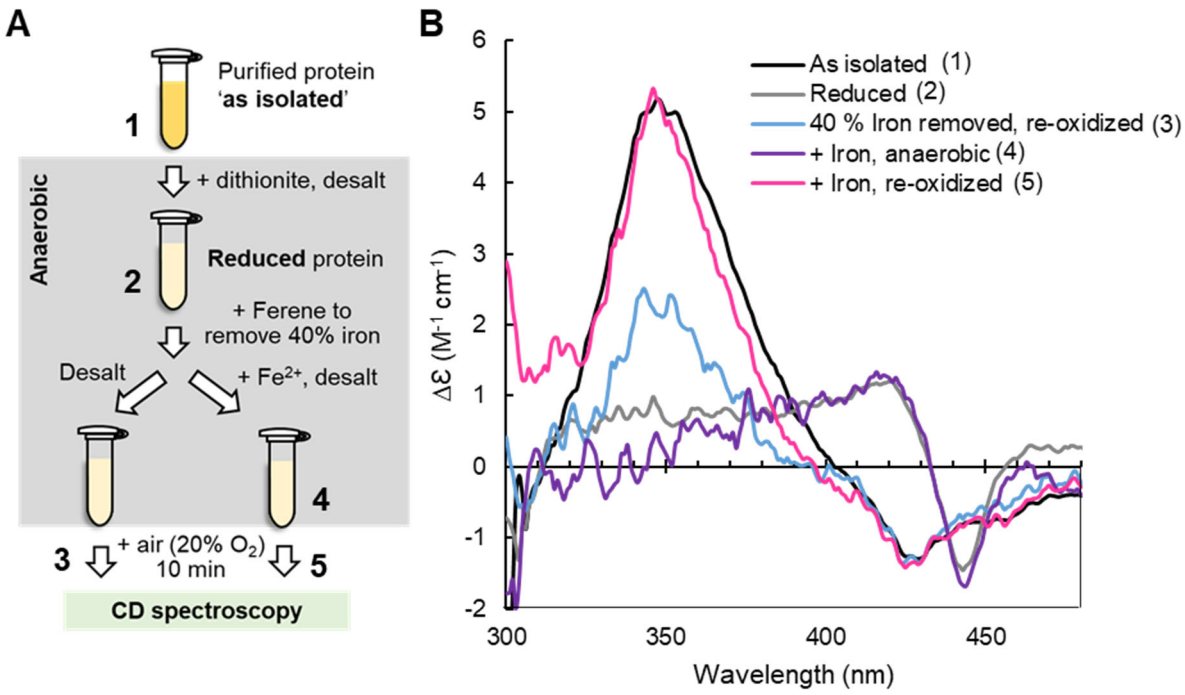

Figure 7. BTSL2-N can be fully reconstituted after partial iron removal.

A. Diagram of the experimental procedures to first remove labile iron and then reconstitute the diiron centres monitored by CD spectroscopy, which only detects protein-bound iron. **B**. CD spectra of purified MBP-BTSL2-N (86 μM) as isolated (black) and after reduction with dithionite and its subsequent removal by desalting (grey). The reduced protein was mixed with a defined amount of Ferene, calculated to remove 40% of the protein-bound iron. Half the sample was desalted to remove Fe^{2+} chelator species, and exposed to O_2 (light blue) to demonstrate the partial removal of protein-bound iron. The other half was mixed with a 3-fold excess of ferrous ammonium sulfate and desalted to remove unbound iron, keeping the protein reduced (purple), followed by exposure to O_2 (magenta). Spectra were adjusted to compensate for dilution by reagent additions and desalting.

371 **DISCUSSION**

372 Physiological and genetic studies point to BTS/L proteins as the main iron sensors that switch
373 off the iron deficiency response in plants, but biochemical studies corroborating this have been
374 lacking. Full characterization of the iron binding and redox properties of the N-terminal Hr-like
375 domain enables us to propose a mechanism by which BTS/L proteins are activated in
376 response to increasing iron levels and oxidative stress (**Figure 8**). The expression of BTS/L is
377 induced by iron deficiency, so when the proteins are initially produced it is likely that the iron
378 binding sites are only partially occupied. Partial iron binding could be important for maintaining
379 the protein in a folded, but inactive, state. As iron levels increase, the diiron centres fill. As and
380 when the cellular environment experiences oxidative stress conditions, rapid oxidation of the
381 diiron centres decreases the lability of the iron and "locks" the protein in its active
382 conformation, which is now able to ubiquitinate its cognate transcription factors, shutting down
383 iron uptake.

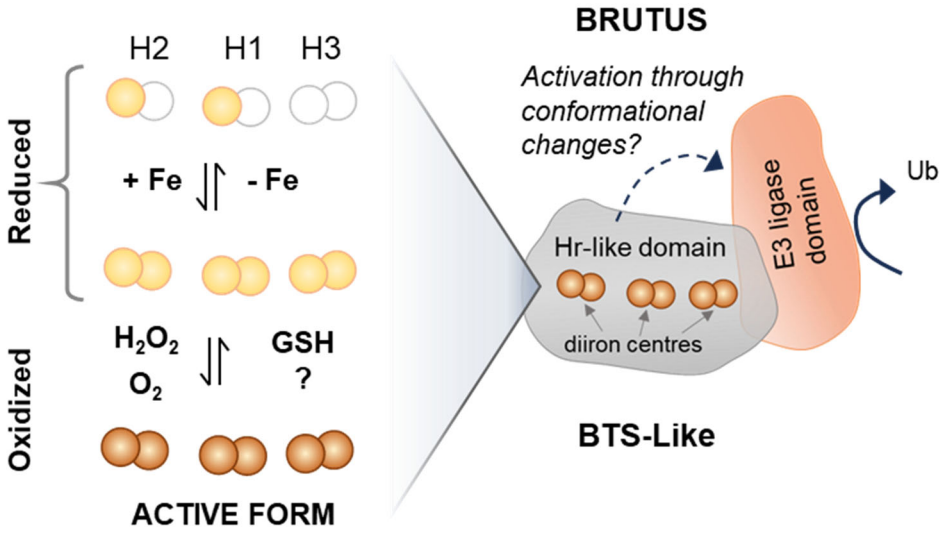

384

385 **Figure 8. Proposed mechanism by which BTS/Ls are activated by iron binding and oxidation.**
386 In a reducing cell environment, iron binding is dynamic, with the diiron centres becoming fully occupied
387 as the iron concentration increases. Oxidation of the diiron centres increases the binding affinity of iron,
388 locking the cofactors in place and leading to activation of the E3 ligase, presumably through
389 conformational changes. Depicted here is the model for BTS with three diiron centres; the H2diiron
390 centre is missing in BTSL2. Fe^{2+} and Fe^{3+} are indicated by light brown and darker brown spheres,
391 respectively.

392 The model makes certain assumptions and also leaves several open questions, to be tested
393 in future experiments. First, the proposed mechanism would allow for distinguishing between
394 iron-induced oxidative stress and oxidative stress from other sources. We believe that iron
395 binding alone is not sufficient to trigger activation. As a multicellular organism, certain cell
396 types experience relatively high intracellular iron concentrations, for example those involved

397 in iron transport. Their role is to pass the iron on to neighbouring cells, and this flux should not
398 be suppressed too easily by BTS/L activation. Second, we believe that reactive oxygen
399 species, rather than O_2, are the physiological oxidants for BTS/L proteins because oxidative
400 stress is a key indicator of excess iron. Kinetic studies of the reaction of BTS/L proteins with
401 different oxidants should be conducted to clarify this.
402 Third, we speculate that the E3 ligase is activated through conformational changes that enable
403 binding of the cognate E2 partner and/or substrate proteins, although other mechanisms are
404 also possible. The observation that expression of the E3 ligase alone (fused to GFP) is more
405 abundant and more active in planta [5] suggests that this is a constitutively active form that lacks
406 the tunable regulatory mechanism and conformational inhibition enabled by the triple Hr-like
407 domain. To investigate this, we need to be able to express and purify sufficient amounts of the
408 full-length proteins, which is currently challenging. However, once achieved, SEC-SAXS could
409 be a valuable technique for studying conformational changes in solution [31]. Fourth, there is
410 the question of why there are always three Hr-like subdomains but variation in the number of
411 diiron centres in BTSL2 and BTS. Does the number of diiron centres align with the dynamic
412 range for iron binding or does it correlate with the responsiveness to oxidative stress? We are
413 in the process of testing ExxxA mutants to individually remove the diiron sites to test the
414 function of these variant proteins in Arabidopsis. Of interest in this respect is the recently
415 identified *bts* mutant in pea, which has a small in-frame deletion in the H1 sequence, predicted
416 to destabilize the diiron centre [32]. The plants show constitutive uptake of iron and hyper-
417 accumulate iron in the leaves, indicating that the E3 ligase domain is not properly activated,
418 despite the presence of an intact H3 diiron centre. Alternatively, the pea BTS protein as a
419 whole may be partially destabilized, consistent with our observations for BTSL2 that the H1
420 site binds iron relatively tightly and may have a structural function.
421
422 The combination of Hr-like domains and E3-ligase activity in the context of regulating iron
423 homeostasis suggest parallels with the mammalian FBXL5 protein [10]. UV-visible spectra of
424 BTSL2 are similar to those of FBXL5 (Figure 3D; [33,34]) and both proteins have a relatively fast
425 autoxidation rate [35-37]. FBXL5 reacted approximately 5 times faster with O_2 than with H_2O_2 [34],
426 whereas H_2O_2 is likely to be the preferred oxidant of BTS/L proteins, as discussed earlier. The
427 diiron centres in BTS/L and FBXL5 have a similar coordination geometry and ligands, based
428 on AlphaFold models compared with the crystal structure of FBXL5 [33]. The ligand binding is
429 asymmetric, with one iron hexa- and the other iron penta-coordinated, which is likely to cause
430 their differential lability as observed in BTS/L proteins. A study on FBXL5 using cyclic
431 voltammetry showed loss of one of the two irons and subsequent reinsertion [34]. Moreover,
432 FBXL5 lost approximately a third of its iron content following reduction and desalting, whereas
433 BTS and BTSL2 retained all bound iron, based on full recovery of the UV-visible spectra

following reduction and reoxidation (Figure 3). This implies that BTS/L proteins have a higher affinity for Fe^{2+} than that of FBXL5.

Iron binding stabilizes the FBXL5 protein, and we believe the same is true for BTS/L proteins, despite a previous report suggesting that Arabidopsis BTS is destabilized by iron [5]. This was based on the observation that BTS protein levels produced in a wheat-germ expression system were diminished in the presence of iron. We have repeated this experiment and found that addition of iron inhibits the transcription or translation in this cell-free system but not the stability of the protein (**Figure S7**). Attempts to remove all iron from oxidized BTSL2-N gradually by increasing the temperature in the presence of an iron chelator resulted in precipitation of the protein. Similarly, unfolding the protein in guanidine hydrochloride, followed by dialysis to remove iron and guanidine, gave precipitates (data not shown). From these experiments and our iron binding studies (Figures 6 and 7), we conclude that the BTS/L N-terminus with partially occupied diiron centres is folded, and that folding is required for stability of the protein.

The need for a thiolate reductant such as β-mercaptoethanol or glutathione to purify stable BTS-N suggests that glutathione plays a physiological role in the iron sensing mechanism. Decreased glutathione levels as a consequence of mutations in the biosynthesis pathway render Arabidopsis seedlings more sensitive to iron deficiency: Key genes involved in iron uptake, including *IRT1* and *FRO2*, were expressed at low levels [38]. It is tempting to speculate that in these mutants the redox equilibrium of the BTS/L proteins is shifted to the oxidized form (Figure 8), leading to increased ubiquitination followed by degradation of the transcription factors of the iron deficiency response. Glutathione was able to partially reduce the BTSL2 N-terminus, but the reaction was slow (Figure S3), consistent with the ability of the Hr diiron sites to sense reactive oxygen species.

The iron-binding and redox properties of the unique triple Hr-like domain of BTS/L proteins shed the first light on the sensing mechanism of these important negative regulators of the iron deficiency response in plants. This will facilitate mutant studies to probe the mechanism in planta, and to potentially modify the system for increasing iron uptake in specific plant tissues for human nutrition (biofortification).

465 **MATERIALS AND METHODS**

466 **Protein expression and purification**

467 Coding sequences of the N-terminal domains of *BTS* (AT3G18290) and *BTSL2* (AT1G18910) were
468 amplified from *Arabidopsis thaliana* cDNA using the following primers listed in Table 1 below and cloned
469 into pMAL-c5x vectors. The BTSL2 E98A and E664A variants were made by site-direct mutagenesis
470 using the listed primers and QuikChange Lightning Site-Directed Mutagenesis Kit (Agilent) according
471 to the supplier's manual.

472 **Table 1.** Primers used in the preparation of recombinant protein expression constructs for this study.

	Forward primer	Reverse primer	Restriction enzymes used
BTSL2 N-term	ACTGCGGCCGCATGGGAGTCG GAGATCCTCTTC	TGACCTGCAGGTTATTTTTCGA ACTGCGGGTGGCTCCA	NotI SbfI
BTS N-term	ACTGCGGCCGCATGGCGACGC CGTTACCAG	TGAGTCGACTTATTTTTCGAAC TGCGGGTGGCTCCAGCATTCA TTAAGCCATTCATCGAA	NotI SalI
2NT-E98A	ATAAGTATCATTCCGCAGCTGC AGATGAGGTTATATTTTCAGC	GCTGAAAATATAACCTCATCTG CAGCTGCGGAATGATACTTAT	-
2NT-E664A	CTGGAAATGCAATCTCATCTGC TGCATCTGAATGTATCTGA	TCAGATACATTCAGATGCAGCA GATGAGATTGCATTTCCAG	-

473

474 The resulting plasmids were used to transform BL21-DE3 Rosetta-pISC cells [39]. The transformed cells
475 were cultured in 4 L Terrific broth containing 0.02% (v/v) glucose at 37 °C to an OD_{600} of 1.1-1.2. Flasks
476 were incubated in an ice bath for 15 min, then induced with 100 μM IPTG, 0.05 % (v/v) DMSO and 50
477 μM ferric ammonium citrate o/n at 16 °C. Cells were harvested and resuspended in 100 mM Tris-HCl,
478 150 mM NaCl, 20 mM β-mercaptoethanol, pH 8.0 with cOmplete EDTA-free protease inhibitor (1 tablet/
479 50 mL). Cells were sonicated while cooled in ice water using 60 cycles of 2 s on, 8 s off at 40% power,
480 and the resulting lysate centrifuged at 20,000 × g for 30 min at 4 °C. The soluble fraction was loaded
481 onto a 5 mL Strep-Tactin XT column (IBA Lifesciences) and washed with 100 mM Tris-HCl, 150 mM
482 NaCl, 20 mM β-mercaptoethanol, pH 8.0. Protein was eluted with 100 mM Tris-HCl, 150 mM NaCl, 20
483 mM β-mercaptoethanol, 50 mM D-biotin, pH 8.0. Removing β-mercaptoethanol from purification buffers
484 after sonication for MBP-BTSL2-N had no effect on the final Fe:protein ratios. Proteins were
485 concentrated using a spin concentrator (MWCO 30 kDa, Pierce). For SAXS experiments, affinity-
486 purified MBP-BTSL2-N-Strep was cleaved using Factor Xa protease (NEB, product no. P9010L) at a
487 concentration of ~2.8 ng/mL for 24 h at 4 °C. Cleaved protein was buffer-exchanged into 10 mM MES,
488 15 mM NaCl pH 6.5 using a spin concentrator (MWCO 30 kDa, Pierce) and BTSL2-N was isolated via
489 size-exclusion chromatography using an S200 26/60 Sephadex column (Cytiva).

490

491

492 **Quantification of iron and other metals**

493 Protein samples which were buffer exchanged into 10 mM Tris-HCl, pH 8.0 and analysed using an
494 iCAP-TQ inductively coupled plasma – mass spectrometer (ICP-MS) from Thermofisher Scientific.
495 Iron in protein samples was also quantified using the colorimetric reagent 3-(2-pyridyl)-5,6-bis(2-(5-furyl
496 sulfonic acid)-1,2,4-triazine, also called Ferene [40]. Protein samples were quantified using the Bradford
497 assay (Protein Assay Dye Reagent, BioRad).

498 **Small-angle X-ray scattering**

499 SAXS data were collected at Diamond Light Source (DLS; Oxfordshire, UK) on beamline 21 in a
500 standard SEC-SAXS experiment. Samples at 1 to 5 mg/ml were applied to a Superdex 200 increase
501 column (Cytiva, Amersham, UK) and run at a flow rate of 0.075 ml/min in 51 mM MES pH 6.5, 75 mM
502 NaCl. Data were recorded at a wavelength of 0.9464 Å using an EigerX 4M detector (Dectris, Baden-
503 Daettwil, Switzerland). Measurements were performed at 15 °C within the q range 0.0045 – 0.34 $Å^{-1}$ (q
504 $= 4\pi\sin\theta/\lambda$; 2θ is the scattering angle, λ is the wavelength) with a sample-to-detector distance of 3.72
505 m. From the SEC-SAXS run of the 5 mg/ml protein sample frames 372-375 were selected, merged and
506 solvent subtracted for data analysis using ScÅtter (https://sibyls.als.lbl.gov/scatter/) IV.d and ATSAS
507 3.2.1 [41]. Calculation of R_g and forward scattering $I(0)$ was performed by Guinier approximation after
508 removing the first 30 data points, The maximum dimension of the particle D_{max} and the $P(r)$ function
509 were estimated using the program GNOM [42]. *Ab initio* envelope models were computed using DAMMIF
510 [18] and overlaid with an AlphaFold2 model [43,44] that was refined against the scattering data using
511 SASREF [45]. The bound iron centres were populated manually via structure superposition with existing
512 PDB entry 2AVK and model editing in the COOT software [46]. Experimental data and models have been
513 deposited in the SAS Biological Data Bank (www.sasbdb.org), accession SASDU79
514 (www.sasbdb.org/data/SASDU79/1g65egyk1i/).

515 **Titrations with O_2 or H_2O_2**

516 The MBP-fusion proteins of the BTSL2 and BTS N-terminal domains were stable at room temperature
517 in a glovebox over a 12 h period, during which redox studies could be performed in an anaerobic
518 environment. Buffer solutions were sparged with N_2 gas for an hour before being left to equilibrate in an
519 anaerobic (<2 ppm O_2) chamber overnight. Protein aliquots were thawed inside the chamber. Gas-tight
520 quartz cuvettes with a 10 mm pathlength (Starna Cells, UK) were used to transfer the protein in and out
521 of the chamber for measurement. Sodium dithionite was prepared in anaerobic buffer and its
522 concentration was determined using an extinction coefficient $\varepsilon_{315} = 8000\ M^{-1}\ cm^{-1}$ [47]. A threefold excess
523 of dithionite was added relative to the protein's iron content and incubated anaerobically. Reduction of
524 the protein was confirmed using circular dichroism measurements made on a Jasco J-810 CD
525 spectropolarimeter to monitor loss of the protein's absorbance peak due to Fe^{3+} at ≈350 nm. Protein
526 was then buffer exchanged on a PD10 desalting column. Aliquots of protein were then titrated with
527 known volumes of H_2O_2 prepared in anaerobic buffer or with aerobic buffer. After each addition of
528 oxidant, a minimum of three minutes elapsed before recording the sample's absorbance or CD
529 spectrum. Absorbance spectra were recorded using a Jasco V550 spectrophotometer.

530

531 **Electron Paramagnetic Resonance**

532 Proteins were degassed, reduced and desalted as above. Proteins were mixed within an anaerobic
533 chamber with the appropriate volume of a supersaturated O_2 solution (prepared by bubbling pure O_2
534 through 100 mM Tris-HCl, 150 mM NaCl, pH 8.0 in a suba-sealed volumetric flask), estimated to be 1.2
535 mM, or a 1.2 mM H_2O_2 solution, and then transferred into EPR tubes. Sealed tubes were removed from
536 the chamber and frozen after the stated reaction times by dropping into methanol cooled in dry ice.
537 Spectra were recorded on a Bruker E500 (X band) EPR spectrometer at 10 K equipped with an Oxford
538 Instruments liquid-helium system. Quantification of paramagnetic species was achieved by comparison
539 of second integrals of the samples' EPR signals with those of a 1 mM Cu^{2+}[EDTA] concentration
540 standard for the mixed-valent Hr sites, or a 35 μM standard of ferric iron binding protein from *Neisseria*
541 *gonorrhoeae* (to measure high-spin mononuclear ferric iron contributing to the g = 4.3 signal) kindly
542 provided by Prof. Dominic Campopiano (University of Edinburgh).

543 **Amplex Red assay**

544 H_2O_2 release from reduced BTS/L proteins was detected using an Amplex Red kit (Thermo Fisher)
545 according to the manufacturer's instructions. Briefly, a 200 μL aliquot of freshly prepared aerobic Amplex
546 Red reaction mixture was mixed with a 200 μL anaerobic aliquot of reduced BTS/L protein, diluted so
547 that the protein-bound iron concentration was 40 μM. The absorbance at 571 nm was used to quantify
548 H_2O_2 based on a calibration curve using 0-37.5 μM H_2O_2.

549 **Iron chelator competition assays**

550 For 'as-isolated' measurements, proteins were thawed in an anaerobic glovebox. For the reduced
551 samples, proteins were treated with dithionite and desalted as described above. Each protein sample
552 was then diluted in a sealed cuvette and single wavelength time courses were recorded using a Jasco
553 V550 spectrophotometer after mixing with colorimetric chelators. Monitored wavelengths were 592,
554 525, and 562 nm for Ferene, 4,4' dipyridyl and ferrozine, respectively. The final concentration of iron in
555 each assay was 75 μM, and 1 mM for each chelator. The percentage iron released was measured
556 relative to calibration curves prepared for each chelator mixed with 0, 10, 25, 50 and 75 μM Mohr's salt
557 anaerobically prepared in 100 mM Tris-HCl, 150 mM NaCl, pH 8.0.

558 **Reconstitution of BTSL2**

559 BTSL2-N (86 μM, 3.8 Fe/ protein) was reduced and desalted as above. Ferene sufficient to remove
560 40% of the iron within the protein was added, and iron removal confirmed by the peak at 593 nm in the
561 absorbance spectrum. A 3x excess of ferrous ammonium sulfate over freshly de-occupied iron binding
562 sites was anaerobically added to the protein, after which the sample was desalted again. The protein
563 was exposed to air for 10 mins in an open Eppendorf with gentle mixing. UV-visible absorbance and
564 CD spectra were recorded after each manipulation. Each CD spectrum represents four spectra to
565 reduce noise on the low intensity signals; for the final sample (air exposed, reconstituted BTSL2) the
566 spectrum was accumulated sixteen times.

567

568

ACKNOWLEDGEMENTS

We thank Dr. Myles Cheesman for use of the CD spectrometer; Graham Chilvers for ICP-MS; Jason Crack for technical advice and discussion; Mark Thornton and Mei Ying Nam (summer students) for protein expression. We acknowledge Diamond Light Source for access to SAXS beamline B21 under proposal MX25108 and beamline scientist Katsuaki Inoue for collecting the data.This work was supported by the Biotechnology and Biological Sciences Research Council, grant awards BB/N001079/1 (to J.R.C, M.F., N.L.B. and J.B.); BB/V015095/1 (to J.P., M.F. and J.B.); BB/V014625/1 (to J.M.B. and N.L.B.); and BB/R013578/1 for the purchase of an ICP-QQQ-MS instrument (J.B. and N.L.B). J.R.C. received additional support from the NextGenerationEU program, award TED2021-130539A-I00; and MCIN/AEI/10.13039/501100011033.

REFERENCES

1. Rodriguez-Celma, J., Chou, H., Kobayashi, T., Long, T.A. & Balk, J. Hemerythrin E3 Ubiquitin Ligases as Negative Regulators of Iron Homeostasis in Plants. *Front Plant Sci* **10**, 98 (2019).
2. Hindt, M.N. et al. BRUTUS and its paralogs, BTS LIKE1 and BTS LIKE2, encode important negative regulators of the iron deficiency response in Arabidopsis thaliana. *Metallomics* **9**, 876-890 (2017).
3. Rodriguez-Celma, J. et al. Arabidopsis BRUTUS-LIKE E3 ligases negatively regulate iron uptake by targeting transcription factor FIT for recycling. *Proc Natl Acad Sci U S A* **116**, 17584-17591 (2019).
4. Kobayashi, T. et al. Iron-binding haemerythrin RING ubiquitin ligases regulate plant iron responses and accumulation. *Nat Commun* **4**, 2792 (2013).
5. Selote, D., Samira, R., Matthiadis, A., Gillikin, J.W. & Long, T.A. Iron-binding E3 ligase mediates iron response in plants by targeting basic helix-loop-helix transcription factors. *Plant Physiol* **167**, 273-86 (2015).
6. Tzafrir, I. et al. Identification of genes required for embryo development in Arabidopsis. *Plant Physiol* **135**, 1206-20 (2004).
7. Alvarez-Carreno, C., Alva, V., Becerra, A. & Lazcano, A. Structure, function and evolution of the hemerythrin-like domain superfamily. *Protein Sci* **27**, 848-860 (2018).
8. Lichtblau, D.M. et al. The Iron Deficiency-Regulated Small Protein Effector FEP3/IRON MAN1 Modulates Interaction of BRUTUS-LIKE1 With bHLH Subgroup IVc and POPEYE Transcription Factors. *Front Plant Sci* **13**, 930049 (2022).
9. Li, Y. et al. IRON MAN interacts with BRUTUS to maintain iron homeostasis in Arabidopsis. *Proc Natl Acad Sci U S A* **118**(2021).
10. Vashisht, A.A. et al. Control of iron homeostasis by an iron-regulated ubiquitin ligase. *Science* **326**, 718-21 (2009).
11. Salahudeen, A.A. et al. An E3 ligase possessing an iron-responsive hemerythrin domain is a regulator of iron homeostasis. *Science* **326**, 722-6 (2009).
12. Wang, H. et al. FBXL5 Regulates IRP2 Stability in Iron Homeostasis via an Oxygen-Responsive [2Fe2S] Cluster. *Mol Cell* **78**, 31-41 e5 (2020).
13. Urzica, E.I. et al. Systems and trans-system level analysis identifies conserved iron deficiency responses in the plant lineage. *Plant Cell* **24**, 3921-48 (2012).

14. Matthiadis, A. & Long, T.A. Further insight into BRUTUS domain composition and functionality. *Plant Signal Behav* **11**, e1204508 (2016).
15. Davidi, L. et al. Pumping iron: A multi-omics analysis of two extremophilic algae reveals iron economy management. *Proc Natl Acad Sci U S A* **120**, e2305495120 (2023).
16. Gommes, C.J., Jaksch, S. & Frielinghaus, H. Small-angle scattering for beginners. *J Appl Crystallogr* **54**, 1832-1843 (2021).
17. Hajizadeh, N.R., Franke, D., Jeffries, C.M. & Svergun, D.I. Consensus Bayesian assessment of protein molecular mass from solution X-ray scattering data. *Sci Rep* **8**, 7204 (2018).
18. Franke, D. & Svergun, D.I. DAMMIF, a program for rapid ab-initio shape determination in small-angle scattering. *J Appl Crystallogr* **42**, 342-346 (2009).
19. Lombardi, A. et al. Retrostructural analysis of metalloproteins: application to the design of a minimal model for diiron proteins. *Proc Natl Acad Sci U S A* **97**, 6298-305 (2000).
20. Pullin, J. et al. Iron Oxidation in *Escherichia coli* Bacterioferritin Ferroxidase Centre, a Site Designed to React Rapidly with H_2O_2 but Slowly with O_2. *Angew Chem Int Ed Engl* **60**, 8361-8369 (2021).
21. Elgren, T.E. et al. Electron transfer associated with oxygen activation in the B2 protein of ribonucleotide reductase from *Escherichia coli*. *Journal of Biological Chemistry* **266**, 19265-19268 (1991).
22. Zhao, G. et al. Iron and hydrogen peroxide detoxification properties of DNA-binding protein from starved cells. A ferritin-like DNA-binding protein of *Escherichia coli*. *J Biol Chem* **277**, 27689-96 (2002).
23. Yamasaki, S. et al. Weak O_2 binding and strong H_2O_2 binding at the non-heme diiron center of trypanosome alternative oxidase. *Biochim Biophys Acta Bioenerg* **1862**, 148356 (2021).
24. Davydov, R.M., Ménage, S., Fontecave, M., Gräslund, A. & Ehrenberg, A. Mixed-valent m-oxo-bridged diiron complexes produced by radiolytic reduction at 77 K studied by EPR. *JBIC* **2**, 242-255 (1997).
25. Hagen, W.R. EPR Spectroscopy of Iron—Sulfur Proteins. 165-222 (1992).
26. Stephens, P.J. et al. Circular dichroism and magnetic circular dichroism of iron-sulfur proteins. *Biochemistry* **17**, 4770-8 (1978).
27. Pellicer Martinez, M.T. et al. Sensing iron availability via the fragile [4Fe-4S] cluster of the bacterial transcriptional repressor RirA. *Chem Sci* **8**, 8451-8463 (2017).
28. Guo, Z. et al. Modulation of MagR magnetic properties via iron-sulfur cluster binding. *Sci Rep* **11**, 23941 (2021).
29. Irving, H. & Mellor, D.H. 1002. The stability of metal complexes of 1,10-phenanthroline and its analogues. Part I. 1,10-Phenanthroline and 2,2'-bipyridyl. *J. Chem. Soc.* **0**, 5222-5237 (1962).
30. Carter, P. Spectrophotometric determination of serum iron at the submicrogram level with a new reagent (ferrozine). *Anal Biochem* **40**, 450-8 (1971).
31. Byer, A.S., Pei, X., Patterson, M.G. & Ando, N. Small-angle X-ray scattering studies of enzymes. *Curr Opin Chem Biol* **72**, 102232 (2023).
32. Harrington, S.A., Franceschetti, M. & Balk, J. Genetic basis of the historical iron-accumulating dgl and brz mutants in pea. *Plant J* (2024).
33. Thompson, J.W. et al. Structural and molecular characterization of iron-sensing hemerythrin-like domain within F-box and leucine-rich repeat protein 5 (FBXL5). *J Biol Chem* **287**, 7357-65 (2012).
34. Wei, Y., Yuan, H., Xu, P. & Tan, X. Redox sensing molecular mechanism of an iron metabolism regulatory protein FBXL5. *Arch Biochem Biophys* **616**, 30-39 (2017).
35. Arkosi, M., Scurtu, F., Vulpoi, A., Silaghi-Dumitrescu, R. & Kurtz, D., Jr. Copolymerization of recombinant *Phascolopsis gouldii* hemerythrin with human serum albumin for use in blood substitutes. *Artif Cells Nanomed Biotechnol* **45**, 218-223 (2017).

36. Arii, H. et al. A novel diiron complex as a functional model for hemerythrin. *Journal of Inorganic Biochemistry* **82**, 153-162 (2000).
37. Crack, J.C. et al. The Di-Iron Protein YtfE Is a Nitric Oxide-Generating Nitrite Reductase Involved in the Management of Nitrosative Stress. *J Am Chem Soc* **144**, 7129-7145 (2022).
38. Shanmugam, V., Wang, Y.W., Tsednee, M., Karunakaran, K. & Yeh, K.C. Glutathione plays an essential role in nitric oxide-mediated iron-deficiency signaling and iron-deficiency tolerance in Arabidopsis. *Plant J* **84**, 464-77 (2015).
39. Grawert, T. et al. IspH protein of *Escherichia coli*: studies on iron-sulfur cluster implementation and catalysis. *J Am Chem Soc* **126**, 12847-55 (2004).
40. Hennessy, D.J., Reid, G.R., Smith, F.E. & Thompson, S.L. Ferene — a new spectrophotometric reagent for iron. *Canadian Journal of Chemistry* **62**, 721-724 (1984).
41. Manalastas-Cantos, K. et al. ATSAS 3.0: expanded functionality and new tools for small-angle scattering data analysis. *J Appl Crystallogr* **54**, 343-355 (2021).
42. Svergun, D.I. Determination of the regularization parameter in indirect-transform methods using perceptual criteria. *Journal of Applied Crystallography* **25**, 495-503 (1992).
43. Jumper, J. et al. Highly accurate protein structure prediction with AlphaFold. *Nature* **596**, 583-589 (2021).
44. Skolnick, J., Gao, M., Zhou, H. & Singh, S. AlphaFold 2: Why It Works and Its Implications for Understanding the Relationships of Protein Sequence, Structure, and Function. *J Chem Inf Model* **61**, 4827-4831 (2021).
45. Petoukhov, M.V. & Svergun, D.I. Global rigid body modeling of macromolecular complexes against small-angle scattering data. *Biophys J* **89**, 1237-50 (2005).
46. Emsley, P. & Cowtan, K. Coot: model-building tools for molecular graphics. *Acta Crystallogr D Biol Crystallogr* **60**, 2126-32 (2004).
47. Dixon, M. The acceptor specificity of flavins and flavoproteins. I. Techniques for anaerobic spectrophotometry. *Biochim Biophys Acta* **226**, 241-58 (1971).